RESEARCH ARTICLE

Analyzing future marine cold spells in the tropical Indian Ocean: Insights from a regional Earth system model

Anand Singh Dinesh[1] | **Pankaj Kumar[1]** | **Alok Kumar Mishra[1]** |
Lokesh Kumar Pandey[1] | **Mukul Tewari[2]** | **William Cabos[3]** | **Dmitry V. Sein[4,5]**

[1]Department of Earth and Environmental Sciences, Indian Institute of Science Education and Research, Bhopal, India

[2]IBM Thomas J. Watson Research Center, Yorktown Heights, New York, USA

[3]Universidad de Alcala, Alcala de Henares, Spain

[4]Shirshov Institute of Oceanology, Russian Academy of Sciences, Moscow, Russia

[5]Alfred Wegener Institute for Polar and Marine Research, Bremerhaven, Germany

Correspondence
Pankaj Kumar, Department of Earth and Environmental Sciences, Indian Institute of Science Education and Research, Bhopal 462066, India.
Email: kumarp@iiserb.ac.in

Abstract

In this study, a future projection of marine cold spells (MCSs) over the tropical Indian Ocean is made using a fully coupled regional Earth system model, namely ROM, under two representative concentration pathways (RCPs): RCP4.5 and RCP8.5. In both RCPs, the future MCS properties have been estimated across three distinct time intervals: the near future (NF; 2010–2039), the middle future (MF; 2040–2069), and the far future (FF; 2070–2099). The future MCS computations were examined with respect to fixed historical baseline periods and varying baseline periods. MCSs were frequent, intense, and prolonged during the historical period. ROM effectively simulated these historical MCS metrics and their trends and outperformed the forcing general circulation model as well as the multimodel ensemble mean of Coupled Model Intercomparison Project phase 5 models. In the future, MCSs will cease to occur in ~13% (4%), ~56% (66%) and ~69% (93%) of the area of the tropical Indian Ocean in the NF, MF, and FF respectively under the RCP4.5 (RCP8.5) scenario using a fixed historical baseline period. This departure of MCSs led to the disappearance of events, first identified over the Arabian Sea in both RCPs. The decrease in net heat flux and increase in wind speed contribute to the genesis and severity of MCS events. Further, during the El Niño regime, the MCS events dramatically decrease due to the basin-wide warming, but during the La Niña phase, the MCS intensity and spatial range increase. This study further investigates the sensitivity of MCSs with the choice of baseline period. Adopting varying baseline periods over time does not result in the disappearance of MCSs but does produce declining trends in MCS activity, highlighting the need for careful consideration in choosing a baseline period.

KEYWORDS
climate, dynamics, ocean, regional and mesoscale modeling, Tropics

1 | INTRODUCTION

Temperature extremes are becoming more frequent and intense with global warming worldwide (Alexander *et al.*, 2006; Seneviratne *et al.*, 2012 and references therein). Hence, much attention has been given to understanding the different spheres of these extreme temperatures in the atmosphere and in the ocean. A marine heatwave (MHW) is a discrete and prolonged period of extremely warm ocean events (Hobday *et al.*, 2016), which

have been studied broadly in recent years. Numerous studies have documented the MHW drivers (Holbrook *et al.*, 2019; Sen Gupta *et al.*, 2020), MHW impacts on biodiversity and ecosystem (Smale *et al.*, 2019), and future projection of MHWs over regional scales using regional models (Darmaraki *et al.*, 2019) and global scales using Coupled Model Intercomparison Project phase 5 (CMIP5) (Oliver *et al.*, 2019) and phase 6 models (Plecha & Soares, 2020). Contrary to MHWs, marine cold spells (MCSs; from here onwards, referred to interchangeably as cold spells or MCSs), defined as a discrete and prolonged period of remarkably cooler ocean water events (Schlegel *et al.*, 2021), have received comparatively less attention despite notable ecological impacts.

Previous studies have used different terminology for describing the cold ocean events that depend on the region and how they impact species. For example, winterkills, degree cooling weeks, cold snaps, and so forth (González-Espinosa & Donner, 2020; Heron *et al.*, 2010; Hurst, 2007). MCSs prominently influence the marine ecosystem by affecting species distribution, declining population, mass mortality, and coral bleaching (Donders *et al.*, 2011; Lirman *et al.*, 2011). Physiologically, an MCS causes a cessation in a species' growth, diminishing fitness and inducing metabolic stress (Burgess *et al.*, 2009). The severity scale of MCS repercussions relies on the combination of multiple factors, such as frequency, intensity, duration, spatial extent, species adaptation, tolerance level, and season of occurrence (Grant *et al.*, 2017; Smith, 2011). Since marine species acclimatize better to cold extremes than to warm extremes (Hicks & McMahon, 2002; Moore, 1976; Morgan *et al.*, 2020), MCS disruptions are generally lighter than those due to MHWs, and their impacts span from none to tolerable. But MCSs become life-threatening during winters. The detrimental consequences are documented as the decline in biomass and mass mortality of fish and invertebrates in the literature (Gilmore *et al.*, 1978; Gunter, 1951; Holt & Holt, 1983; Mceachron *et al.*, 1994; Wells *et al.*, 1961). On the other hand, the beneficial importance of MCSs includes removing non-endemic species (Wells *et al.*, 1961), augmenting primary production (Chiswell & O'Callaghan, 2021), and relieving low thermally tolerant species in the warming ocean (Mintenbeck, 2017; Veytia *et al.*, 2020).

The most comprehensive study on global MCSs is that of Schlegel *et al.* (2021), covering the intense MCSs over Florida in 2003, the Taiwan Strait in 2008, and the 2013–2016 Atlantic cold blob. Although the global pattern of MCSs from the satellite era to date is known, how global warming is going to change the MCSs in the future is still unclear. To the best of our knowledge, at the time of writing this article, no future projection of MCSs is

available covering a global or regional scale. Considering the tropical Indian Ocean (TIO), which is the region of our study, a substantial reduction in the frequency, intensity, duration, and extension of MCSs is expected as TIO is warming at a much faster rate (1°C) than the global ocean (0.7°C) from 1951 to 2015, as shown in the Sixth Assessment Report of the Intergovernmental Panel on Climate Change (IPCC; IPPC *et al.*, 2019).

Generally, regional Earth system models (RESMs) are preferred over coupled general circulation models (GCMs) to better understand the regional-scale mesoscale process, as they efficiently resolve the small-scale processes and their interaction among the Earth system components (Giorgi, 2019; Kumar *et al.*, 2014a; Kumar *et al.*, 2014b; Kumar *et al.*, 2023; Mishra *et al.*, 2021a; Mishra *et al.*, 2021b; Mishra *et al.*, 2023; Pandey *et al.*, 2021). Additionally, they can be run at high resolution with optimized computational cost. Therefore, this article attempts to provide the first ever future projection of MCSs over the TIO using a fully coupled RESM, namely ROM. Also, this study endeavors to quantify how MCS distribution, intensity, and duration will change from historical periods and how it will look in the future.

2 | MATERIALS AND METHODS

2.1 | Model description and component

This study has employed a high-resolution RESM, namely ROM, that comprises three components: atmosphere, ocean, and terrestrial hydrology (Sein *et al.*, 2015; Sein *et al.*, 2020; Sein *et al.*, 2022): REMO is the regional climate model used for the atmospheric component (Jacob *et al.*, 2001; Jacob & Podzun, 1997), the Max Planck Institute Ocean Model (MPIOM) is used for the oceanic component (Jungclaus *et al.*, 2013), and additionally the global Hydrological Discharge (HD) model (Hagemann & Dümenil, 1997) is also included. Note that all the model components of ROM, except REMO, are global.

REMO is a three-dimensional hydrostatic atmospheric model that is regionally constituted over the Coordinated Regional Climate Downscaling Experiment (CORDEX)-South Asia domain and uses temperature, pressure, wind, water vapor, and cloud content from the CMIP5 model (namely, MPI-ESM-LR) as a lateral boundary forcing. REMO is integrated at 0.44° (∼50 km) with 27 hybrid vertical levels and utilizes a rotated Arakawa C-grid that efficiently handles horizontal discretization (Sein *et al.*, 2015).

The MPIOM is a primitive equation global ocean model based on hydrostatic and Boussinesq assumptions. It is devised on an Arakawa curvilinear C-grid with 40

vertical levels (Marsland *et al.*, 2003; Sein *et al.*, 2015). The MPIOM is unified with a dynamic/thermodynamic sea-ice model based on viscous–plastic rheology following Hibler (1979) and the Hamburg Ocean Carbon Cycle biogeochemistry model. For inferring flow across steep topography, MPIOM has a bottom boundary-layer parametrization (Marsland *et al.*, 2003). In this study, MPIOM is implemented with a varying horizontal grid employing a higher resolution over the target area (Indian Ocean) of ∼50 km, varying up to ∼5 km over the coastal area of the Arabian Sea (AS) and the Bay of Bengal (BoB).

The HD model, which is run as a REMO module, covers the globe with uniform horizontal resolution (0.5°) to simulate the lateral freshwater fluxes. The model parameters are the topography gradient, its length and slope, the lake area, and the wetland fraction of the individual grid box.

The model components have been coupled using the Ocean–Atmosphere Sea Ice Soil coupler that exchanges the information between REMO-HD-MPIOM at 1 day intervals, whereas information is shared every 3 hr between REMO and MPIOM. More details about the model integration and detailed dynamics can be obtained from the literature (Dubey & Kumar, 2023; Kumar *et al.*, 2022; Mishra *et al.*, 2021b; Mishra *et al.*, 2022; Saharwardi *et al.*, 2022; Sein *et al.*, 2015; Sein *et al.*, 2020; Sein *et al.*, 2022).

After ca. 100 years of spin-up, three simulations were carried out using ROM: one for the past climate (1950–2005) and the other two for the future projection (2006–2099) using two representative concentration pathways (RCP) emission scenarios (RCP4.5 and RCP8.5). All simulations were at a horizontal resolution of 0.44° × 0.44° over the CORDEX-South Asia domain using CMIP5 model MPI-ESM-LR (hereafter interchangeably referred to as ESM or MPI-ESM-LR) data as boundary condition. Notably, MPI-ESM-LR is among the best CMIP5 models that showed better warming trends over the TIO (Li & Su, 2020). The implication of this can be inferred as a better input file to the RESM will yield good simulated fields.

For this study, 1976–2005 (30 years) is taken as a historical period. Also, a subset of historical data covering the period of 1982–2005 has been used to evaluate model simulation and is called the evaluation period. The primary reason for selecting this period for evaluation is due to the availability of the National Oceanic and Atmospheric Administration's (NOAA's) Optimum Interpolation Sea Surface Temperature (OISST) data from 1982 onwards. The ROM data covering 2006–2099 is classified into three time slices, each of 30 years; namely, the near future (NF; 2010–2039), the middle future (MF; 2040–2069), and the far future (FF; 2070–2099) for both RCPs. This classification of time-frame is specifically chosen for this study domain, as the future projection of heatwaves, drought, and precipitation (Dubey *et al.*, 2021; Kumari & Kumar, 2023; Saharwardi *et al.*, 2022) have nearly chosen the same time-frame. Additionally, these periods are also used in the IPCC reports (Seneviratne *et al.*, 2021). Hence, this time-frame selection will ensure consistency across disciplines.

2.2 | Observation datasets

This study uses the daily sea-surface temperature (SST) data available at 0.25° from NOAA's OISST datasets (Reynolds *et al.*, 2007) as observation data. This dataset includes observations from different platforms, such as Advanced very high-resolution radiometer satellite retrievals, buoys, ships, and Argo floats. Daily OISST datasets having global coverage are available from September 1981 to date. The MCS characteristics from OISST datasets have been calculated at each TIO grid from 1982 to 2005 (evaluation period) to examine the model performance in capturing MCSs.

2.3 | CMIP5 multi-model ensemble mean

ROM has a better depiction of the physical and dynamical processes of Earth system components (i.e., atmosphere, ocean, and hydrological components) along with the full biogeochemical cycles that gives a better representation to suitably simulate the regional climate in comparison with CMIP5, their ensemble and standalone regional climate models which have been reported in our previous studies (Dubey & Kumar, 2023; Kumar *et al.*, 2022; Mishra *et al.*, 2021b; Saharwardi *et al.*, 2022). Hence, in line with those, this study also compares the performance of ROM with the ensemble mean of CMIP5 models for MCS characteristics to further depict its robustness. Therefore, the multimodel ensemble (MME) mean of four CMIP5 models (MPI-ESM-LR, NorESM1-M, CMCC-CMS, FGOALS-s2) for the evaluation period (1982–2005) has been taken. These four models were selected explicitly because they demonstrate better warming trends in SST over the Indian Ocean (Li & Su, 2020) out of 37 CMIP5 models.

2.4 | MCS definition and its estimation

MCS is defined as a discrete, prolonged, and anomalous cold-water event over a specific location (Schlegel *et al.*, 2021). An MCS event is reported when the SST

is below the seasonally varying 10th percentile threshold for 5 days or more (Schlegel *et al.*, 2021). The seasonally varying threshold permits MCSs to occur in every season of the year, even in summer.

Historical and future (NF, MF, FF) cold spells were detected at each grid of the TIO by calculating the time series of daily SST anomalies relative to the 30-year historical baseline period's SST (1976–2005). Previous reports (e.g., Oliver *et al.*, 2021; Sen Gupta *et al.*, 2020; Smith, 2011) have argued using a fixed historical baseline period to study the future extremes because it has an ecological implication. Currently, the capacity of the ocean ecosystem to adjust to cold stress with acute to chronic impacts is largely known, which is why future changes in MCS intensity can be easily translated into probable future effects on the ecosystem (Smith, 2011). Other than that, it is general practice in climatology studies to utilize a fixed historical baseline period to demonstrate overall changes in future extremes. Various studies (Darmaraki *et al.*, 2019; Frölicher *et al.*, 2018; Oliver *et al.*, 2019) have utilized historical threshold values for studying the future oceanic extremes using GCMs and RESMs. Additionally, the fixed-baseline approach is widely adopted in the IPCC reports, such as in the special report *The Ocean and Cryosphere in a Changing Climate* (Pörtner *et al.*, 2019). Therefore, by choosing this fixed historical baseline period, consistency with the earlier studies/reports will be maintained, and confusion will be avoided. Hence, we primarily utilized the historical baseline period for the future assessment of cold spells. However, we acknowledge that a fixed baseline period does not take into account the warming of the oceans over time and may lead to some artefactual MCS metrics in the future (Amaya *et al.*, 2023), as these extremes have a high dependence on the selected baseline period (Amaya *et al.*, 2023; Dinesh *et al.*, 2023; Oliver *et al.*, 2021). Therefore, to avoid any potential bias from the selection of baseline period, this study utilizes the near, middle and far future threshold values for studying the corresponding period's MCS, which is primarily done to analyze the scale of potential changes.

For understanding MCS characteristics, the following MCS metrics have been used: (a) number of events; (b) maximum intensity, which refers to the maximum temperature anomaly; (c) duration, which is defined as the mean annual duration of events; and (d) the different categories of MCS are computed. When the difference between the climatological mean and climatological 10th percentile, which is a threshold used for MCS identification, is 1–2 times, then it is categorized as Moderate, 2–3 times is categorized as Strong, 3–4 times is categorized Severe, and >4 is categorized as Extreme (Schlegel *et al.*, 2021).

2.5 | Dissolution dates

The frequency and intensity of MCS globally are decreasing due to ocean warming, except in specific regions such as the Southern Ocean and the eastern equatorial Pacific (Schlegel *et al.*, 2021). To identify this pattern, we computed the last occurrence of an MCS over each grid point within the TIO. This final occurrence marks what we refer to as the "disappearance date"—a point after which no further MCS events are anticipated in that area. Understanding the disappearance date for MCS allows us to pinpoint regions within the ocean experiencing a more rapid decline in these weather systems. This information is valuable, offering insights for optimizing local response planning and proving relevant in diverse ecological studies.

2.6 | Mixed-layer heat budget

The atmospheric parameters short-wave radiation (SWR), long-wave radiation (LWR), latent heat flux (LHF), sensible heat flux (SHF), and wind speed (WS), along with oceanic parameters like zonal advection (ZADV), meridional advection (MADV) and vertical velocity, have positive and negative feedbacks on SST (Saranya *et al.*, 2022; Srivastava *et al.*, 2016 and references therein). Therefore, these parameters can regulate the conditioning of MCSs. Generally, the ZADV, MADV, and vertical velocity are derived from mixed-layer heat budget analysis. The u, v, and w current data in our model are available on a monthly scale, hence limiting the mixed-layer heat budget analysis to be done on a monthly scale. It is important to note that an MCS, being a mesoscale phenomenon with a typical duration of a few days to a few weeks, may not be directly influenced by these oceanic parameters available at a monthly scale in an explicit manner. Instead, this mixed-layer heat budget analysis will provide a comprehensive picture of how these atmospheric and oceanic factors lead to future rise in the ocean SST and, hence, indirectly influence MCSs, resulting in the disappearance of cold spells. That said, it is well established that decreasing trends in MCSs are primarily driven by a rise in mean SST (Wang *et al.*, 2022) rather than variability in this atmospheric and oceanic component. However, it will still be interesting to note how this atmospheric and oceanic component may exert some influence on MCSs in the future.

Equation (1) represents the processes in the mixed-layer heat budget, where T_{ml} is the mixed-layer temperature (Vialard *et al.*, 2001; Vialard & Delecluse, 1998):

$$\delta T_{ml} = -\frac{1}{h}\int_{-h}^{0} u\partial_x T\, dz - \frac{1}{h}\int_{-h}^{0} v\partial_y T\, dz - \frac{1}{h}\int_{-h}^{0} D1(T)$$

$$-\frac{1}{h}(T_{\mathrm{ml}} - T_{-h})(w_{-h} + \partial_t h)$$

$$-\frac{1}{h}\left[k_z \partial_z T\right]_{-h} + \frac{Q_s(1 - F_{-h}) + Q_{\mathrm{ns}}}{\rho_o C_p h}. \qquad (1)$$

The first two terms on the right are the zonal and meridional temperature advection respectively. The third term is diffusion, represented by D1. Later, the lateral mixing process and the vertical exchange of heat between the mixed layer and the subsurface ocean are represented by terms 4 and 5 respectively. The final term on the right is atmospheric heat flux forcings. In the equation, the temperature is denoted by T, and the h is a time-varying model mixed-layer depth. Further, k_z, Q_s, and Q_{ns} are the vertical mixing coefficients for the tracer, solar, and non-solar components of surface heat flux respectively. The solar radiation that penetrates to depth h is F_{-h}. ρ_o and C_p are the seawater reference density and volumic heat capacity respectively. All estimated heat budget components have been converted to the same unit of measurement (°C·day^{-1}).

2.7 | Climate modes

The large-scale climate mode El Niño–Southern Oscillation (ENSO) and the Indian Ocean Dipole (IOD) have a prominent role in altering the SST of the TIO (Du *et al.*, 2009; Saji *et al.*, 1999; Sayantani & Gnanaseelan, 2015). During the positive phase of ENSO (i.e., during El Niño), the western Indian Ocean shows a warmer anomaly. During the negative phase (i.e., La Niña), most parts of the Indian Ocean experience a cooler anomaly (Benthuysen *et al.*, 2014; Roxy *et al.*, 2014; Swapna *et al.*, 2014). During the positive (negative) phase of the IOD, anomalous warming (cooling) in the western (southeastern) TIO is evident. Therefore, both climate modes might affect the preconditioning, generation, and reinforcement of MCS conditions over the TIO. Hence, for ENSO representation, the Oceanic Nino Index (ONI) is utilized. The SST anomalies in ONI are calculated over the (5 N–5°S, 170 W–120 W) box using a 3-month running mean. El Niño (La Niña) is declared when the anomalies go beyond +0.5°C (−0.5°C) for five consecutive months. The ONI has been calculated with respect to the historical climate (1976–2005), which is also the baseline for estimating future cold spells. For the IOD, the Dipole Mode Index (DMI) is estimated as the monthly SST difference between the western TIO (50°E–70°E and 10°S–10°N) and the southeastern TIO (90°E–110°E and 10°S–0°N) boxes. For the DMI, a 3-month running average was used to smooth the time series. When the DMI is higher (lower) than +0.4°C (−0.4°C) for at least

3 months, positive (negative) IOD events occur (Cahyarini *et al.*, 2021; Tobin, 2020).
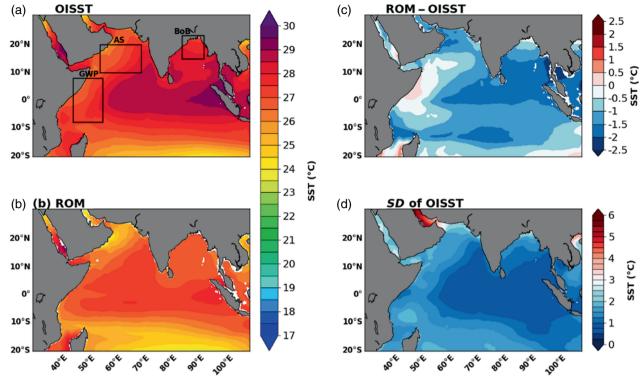
3 | RESULT AND DISCUSSIONS

3.1 | Model evaluation

Before projecting the future cold spell characteristics, verifying the model performance in simulating the observed cold spells and its deriving parameter, SST, is mandatory. Therefore, to develop confidence in model simulation, various validations have been done: (a) comparison of the mean SST features; (b) a comparison of the MCS metrics; (c) comparison of trends in MCS metrics; and (d) statistical indices for MCSs in between observation and ROM.

From Figure 1a,b, it can be observed that ROM closely resembles OISST in producing mean SST. It delineates the region of low and high SST with some systematic biases. The bias map in Figure 1c shows cold bias over most areas, with substantial spatial variability. The ROM underestimates the mean SST and shows maximum negative bias around the South China Sea, Gulf of Martaban, Gulf of Oman, parts of the equatorial Indian Ocean, and Madagascar. ROM depicts a slight positive bias limited to some areas of the Great Whirlpool (GWP) region, Mozambique Channel region, and various regions covering the 110°E–120°E strip of the TIO domain. Over the majority of the TIO, the biases present in the ROM are less than the *SD* of observations, as shown in Figure 1d.

Figure 2a shows the MCS metrics computed from the OISST, ROM, ESM, and MME. It is evident from the OISST-derived MCS (Figure 2a1) that most of the TIO region has faced more than two events per year except the AS (55°E–70°E, 10°N–20°N) and GWP (45°E–56°E, 8°S–8°N). The BoB (85°E–93°E, 15°N–23°N) and the Sumatra region have a greater number of events. In general, the eastern TIO had more frequent MCSs than the western TIO during 1982–2005. Notably, the intensity of the cold spells is generally reported with a minus sign (Schlegel *et al.*, 2021). In observations, the highly intense MCSs are found near the coast (Figure 2a5), over the AS, BoB, and Sumatra region, for instance, extending to many kilometers from the shorelines. In contrast, in the southern TIO, maximum intensity is generally higher and found primarily in the region bounded by 0° to 10°S over shorelines and in the open ocean (Figure 2a5). The GWP region is an upwelling region that brings cold water from the bottom to the surface; therefore, a higher magnitude of MCS intensity is perceivable. Notably, although the number of MCS events in the AS is less than that of the BoB the intensity of events is quite analogous. The annual duration of MCSs in observation (Figure 2a9) is more pronounced in
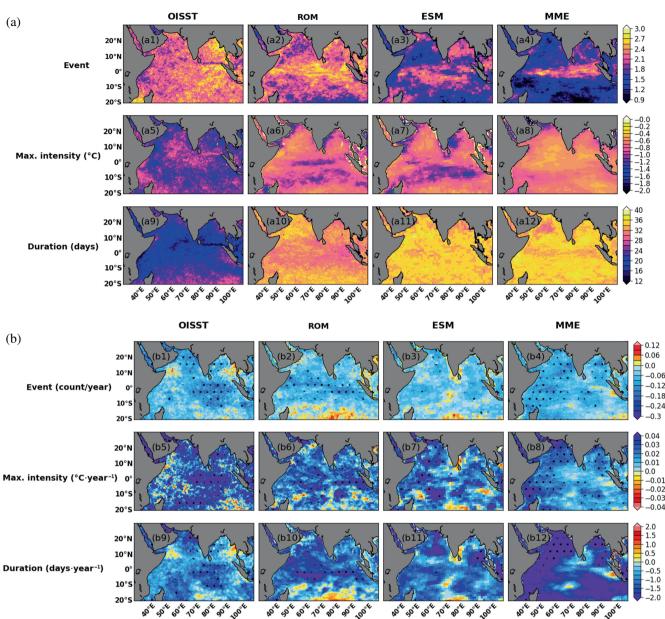
FIGURE 1 (a) Mean sea-surface temperature (SST) in the observation. (b) Mean SST in the ROM. (c) Mean SST bias present in the ROM. (d) The *SD* of SST in the observation. [Colour figure can be viewed at wileyonlinelibrary.com]

the southern TIO, primarily between 10°S and 20°S. At the same time, the eastern AS, BoB, and Sumatra regions have shown more prolonged MCSs (Figure 2a9).

ROM has simulated more cold spell events, especially in the region around the Equator that extends from 10°N to 10°S, whereas fewer events have been detected in the BoB, AS, and the region below 15°S (Figure 2a2). Meanwhile, ESM and MME have detected many fewer MCS events over the entire TIO (Figure 2a3,a4). In ROM, an underestimation in the intensity of cold spells is perceived over the TIO (Figure 2a6). This underestimation ranges from 0°C to 1°C over the majority of the TIO. Similar to ROM, ESM and MME also underestimate the MCS intensity (Figure 2a7,a8). The underestimation of MCS intensity in MME is much higher than in ROM and ESM. The annual duration of MCSs is reported to be higher in ROM, ESM, and MME (Figure 2a10–a12), showing a tendency to produce extended MCS durations. In comparison with the ESM and MME, the overestimation in ROM is smaller.

In investigating the trends of MCS metrics it is also essential to depict the zone where an increase/decrease in MCS metrics is observed. Therefore, demonstrating the model performance in simulating the trend is essential to build confidence in the reliable projection. It should be carefully noted that MCS intensities are represented with negative numbers, and hence, a positive trend in MCS intensity over time indicates a weakening, whereas for the

event and duration, a positive trend means strengthening of an MCS. Figure 2b shows the trends in the MCS metrics from the observation, ROM, ESM, and MME. It can be easily perceived that ROM and ESM bear a parallel resemblance with observation in reproducing trends, along with some regional discrepancies. MME has a better representation of events and intensity trends, but duration trends are decreasing more drastically than observed over the western TIO. Primarily, all MCS metrics demonstrate a decreasing trend.

To provide a more comprehensive perspective, we have employed statistical indices to assess the model performance in measuring cold spells. The statistical analysis—in terms of pattern correlation coefficient (CC), root-mean-square error (RMSE), and skill score (SS)—for MCS metrics are summarized in Table 1, which shows the superior performance of ROM against forcing ESM and MME. ROM bears a good resemblance in simulating the MCS metrics with a high pattern CC. The SS is the ratio between the RMSE of the model to the *SD* of observation, and it has been previously used (Dwivedi *et al.*, 2018; Dwivedi *et al.*, 2019; Pandey & Dwivedi, 2021; Srivastava *et al.*, 2016) in determining the model's potential. SS < 1 demonstrates the fit of model simulation. The SS for all MCS metrics of ROM is <1, indicating the quality of ROM simulations. Table 1 includes the statistical indices of ROM for all MCS metrics.

FIGURE 2 (a) Marine cold spell metrics and (b) their trends in the observation (Optimum Interpolation Sea Surface Temperature [OISST]), ROM, Earth system model (ESM), and multimodel ensemble (MME) during the evaluation period (1982–2005). Stipples represent the 95% significance level. [Colour figure can be viewed at wileyonlinelibrary.com]

The various cross-validations of ROM for historical simulation confirm ROM's satisfactory performance in reproducing observed MCSs. Thus, it can be used for the future projection of MCSs over the TIO.

3.2 | Future MCS metrics with fixed baseline period

The future MCS characteristics over the TIO are calculated with respect to the historical baseline climatology (1976–2005). Figure 3a,b shows the future MCSs in the RCP4.5 and RCP8.5. It can easily be perceived from

Figure 3a,b that the proportion of the TIO surfaces experiencing an MCS is declining rapidly with the progression of time. In RCP4.5 (RCP8.5) during the NF, the proportion of the TIO surface experiencing an MCS will drop by ~13% (4%), whereas in the MF it drops further to ~56% (66%), and finally, during the FF the areas without any MCS will cover ~69% (93%) of the TIO. In the NF with both RCPs, the number of events was higher than during the MF and FF periods; the more frequent events persist over the northern AS, western BoB, and the Southern Hemisphere. During the NF in both RCP scenarios, the MCS intensity decreases by about four times over the northern AS, western BoB, and Southern Hemisphere, whereas over

TABLE 1 Statistical indices of regional Earth system model ROM, Earth system model (ESM), and multimodel ensemble (MME) compared against the observation (Optimum Interpolation Sea Surface Temperature [OISST] dataset) for marine cold spell metrics. [Colour table can be viewed at wileyonlinelibrary.com]

	ROM			ESM (MPI-ESM-LR)			MME		
	Event	Max. intensity	Duration	Event	Max. intensity	Duration	Event	Max. intensity	Duration
Correlation coefficient	0.88	0.86	0.90	0.85	0.83	0.87	0.84	0.76	0.88
Root-mean-square error	0.53	0.39	9.59	0.62	0.42	11.84	0.74	0.48	11.84
Skill score	0.51	0.67	0.90	0.60	0.72	1.11	0.71	0.84	1.11

FIGURE 3 Marine cold spell metrics in the future (near future [NF], middle future [MF], and far future [FF]) using the (a) RCP4.5 and (b) RCP8.5 scenarios. [Colour figure can be viewed at wileyonlinelibrary.com]

FIGURE 4 Disappearance date of marine cold spells (MCSs) in the future with the (a) RCP4.5 and (b) RCP8.5 scenarios. (c) Proportion of the tropical Indian Ocean (TIO) losing MCS events with time. [Colour figure can be viewed at wileyonlinelibrary.com]

other parts of the TIO it shrinks by about eight times with respect to the historical period. Both RCP scenarios follow these intensity drops up to the FF, and most of the region experiences mild MCSs with only −0.2°C. Similarly, the duration of MCSs is declining consistently in all the time slices in both RCPs. The maximum duration of an MCS event during the NF is confined to the Southern Hemisphere and the Northern AS in both RCPs (~18 days), whereas over most of the TIO, it is ~6–8 days. In general, the MCS events, intensity, duration, and spatial extent all decrease with time.

Interestingly, the presence of cold spells, even in the FF period over limited areas of the northern AS, western BoB, and Southern Hemisphere region of the TIO in both RCPs suggests that the regional atmospheric/oceanic processes have a crucial role in generating and maintaining the MCS events over some TIO areas.

In both RCPs, the uninterrupted withdrawal of the MCS event and reduction in its spatial extent indicate the dissolution of MCSs from the TIO. Hence, the date of dissolution of MCSs at each grid is computed and shown in Figure 4a,b for RCP4.5 and RCP8.5. Strong spatial variability is visible in the dissolution date of the MCS events, with its first disappearance over the AS and GWP in both scenarios. The eastern coast of India, the northwestern AS,

and the region in the Southern Hemisphere show delayed dissolution in RCP4.5, and the same region in RCP8.5 has also shown delayed dissolution compared with other TIO locations. Because of the greater warming in RCP8.5, cold spells are expected to disappear earlier in RCP8.5 than in RCP4.5. Approximately 55% of the TIO is projected to lose their MCSs sooner in RCP8.5 than in RCP4.5. Figure 4c shows the proportion of the TIO without MCSs as time passes. The proportion of the TIO without MCSs shows a significant increase in both RCPs after 2015. Interestingly, up to 2030, the proportion of the TIO losing MCS events is relatively larger in RCP4.5. However, in RCP8.5, after 2030, a continuous increment in the proportion of the TIO losing MCSs is noticeable. In the last decade of the century, ~96% (89%) of the TIO will lose its MCSs under the RCP8.5 (RCP4.5) scenario.

3.3 | Driver responsible for the genesis and cause of future MCS dissolution with a fixed baseline period

The AS, BoB, and GWP show noticeable changes in the cold spell properties from historical time to the future, and hence these specific regions were selected for exploring
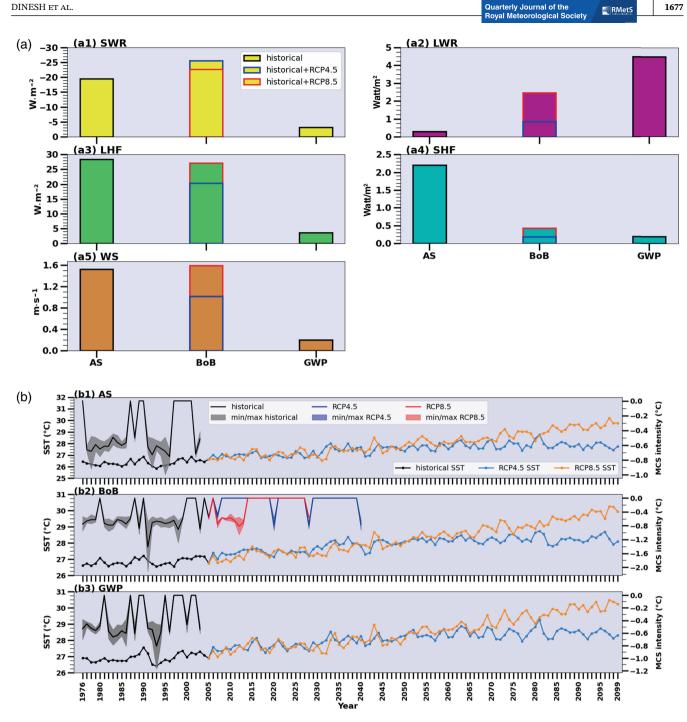
FIGURE 5 (a) Anomaly in the atmospheric parameters 5 days before a marine cold spell (MCS). (b) Evolution of mean annual sea-surface temperature (SST) and mean annual MCS intensity over the Arabian Sea (AS), Bay of Bengal (BoB), and Great Whirlpool (GWP). The black, Dodger blue, and orange lines with dots represent SST in the historical, RCP4.5, and RCP8.5 period respectively, whereas the black, blue, and red lines indicate the MCS intensity in the historical, RCP4.5, and RCP8.5 period respectively. SWR: short-wave radiation; LWR: long-wave radiation; LHF: latent heat flux; WS: wind speed. [Colour figure can be viewed at wileyonlinelibrary.com]

the role of dynamical and thermodynamical properties of environmental parameters in the genesis of MCSs. In this regard, we have taken the area average SST over the AS (55°E–70°E, 10°N–20°N), BoB (85°E–93°E, 15°N–23°N), and GWP (45°E–56°E, 8°S–8°N) to determine the MCSs and then explore the genesis of MCSs from daily data of thermodynamical terms (SWR, LWR, LHF, and SHF) and

dynamical terms (WS) from the ROM model. Figure 5a shows the mean change in the dynamical and thermodynamical terms 5 days prior to MCS genesis. The reduction in the SWR, increment in the LWR, evaporative cooling (LHF), and heat flow from the surface to atmosphere lead to a relatively cooler SST and favor the genesis of an MCS over the AS, BoB, and GWP; in addition to that, the WS

is found to be increased. The increased WS brings more turbulence and vertical mixing that causes increased heat dissipation from the upper surface to the lower layers. It is imperative to note that, in general, the coherence impacts of dynamical and thermodynamical changes lead to the generation of cold spells; nevertheless, the role of individual terms varies at each location. For example, over the GWP, the role of LWR is more prominent than the other parameters. Over the AS, which is warming at an alarming rate, the magnitude of change in dynamical and thermodynamical parameters is sufficiently higher to generate an MCS event. Over the BoB, the SHF is less responsible for MCSs, whereas other parameters contribute significantly and have varying magnitudes depending on the RCP.
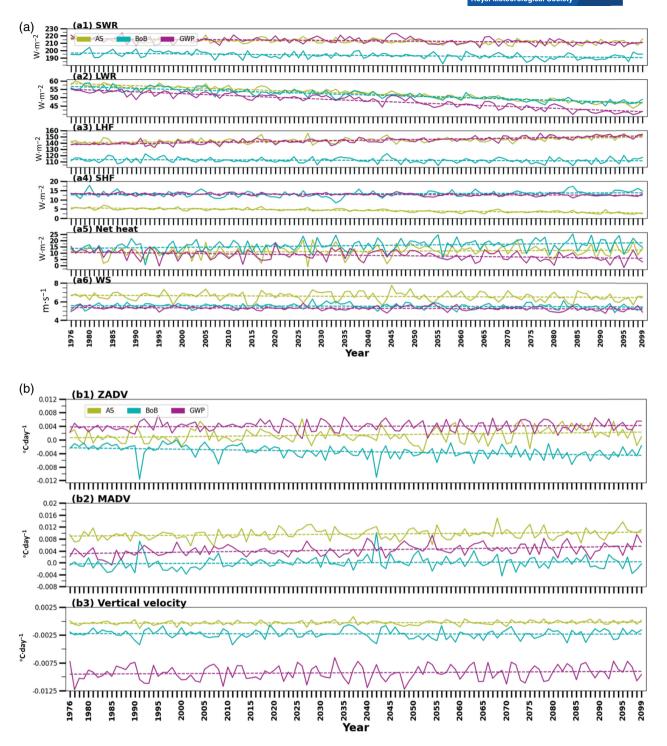
Figure 5b shows the yearly mean SST and MCS intensity from historical times to the future over all three locations. The solid black, blue, and red colors (gray, light blue, and light red colors) demonstrate the mean MCS intensity (spread of MCS intensity) respectively in historical times, RCP4.5, and RCP8.5. The dotted black, Dodger blue, and orange demonstrate the annual mean SST in historical times, RCP4.5, and RCP8.5 respectively. Over the AS and GWP, the frequency of MCS events ceases in the historical period; however, over the BoB, MCSs will still be present in both RCPs in the future. The MCSs over the BoB with RCP8.5 were present until 2027, whereas they were present up to 2040 with RCP4.5. The mean annual SST over all three locations is warming, with a larger magnitude of SST in RCP8.5. The mean SST at each location increases with time, implying that the daily time series of SST will be above the 10th percentile of the historical threshold value, and thus no MCSs will be detected.

Future results from the RCP8.5 scenario show a marginal fall in SWR, LHF (except the AS and GWP), and SHF (except the BoB); however, it is clear that LWR has significantly decreased (Figure 6a). In LWR, the slope of decline is found to be the greatest. Therefore, an overall increase in net heat is expected, which helps to partially explain the increasing SST in the future; however, the net heat over the GWP is found to decrease slightly, indicating other oceanic processes are also likely to contribute to the rising SST. In addition, a further rise in SST is caused by a drop in WS strength. One may also argue that over the GWP the LWR, which has the greatest impact on the MCS genesis, is declining at a higher rate (slope: -0.1104) than at the other locations (slope: -0.0988 for AS, -0.0802 for BoB) and thus may have a significant impact on MCS dissolution relative to other parameters in the GWP. Similar cases with other parameters can also be valid for other locations. Figure 6b, looking into the oceanic parameters, shows that the increasing trend of ZADV and MADV are accumulating more heat and pushing SST higher in the future compared with what was historically observed. The vertical velocity causes cold water from the bottom to rise to the surface, which helps to lower the SST; therefore, its magnitude is often negative. In the future, this role of vertical velocity in cooling the SST is losing its strength. That is, the vertical velocity in the future has a tendency to upwell water that is somewhat warmer than it was in the past. The ocean's subsurface warming might bring this on. As shown in Figure 6b3, the trend of vertical velocity over all locations is shifting towards less negative values. With RCP4.5, similar changes in atmospheric and oceanic parameters were achieved, albeit obviously with a smaller magnitude that has no bearing on the main finding.

3.4 | MCS relation to ENSO and the IOD

Figure 7a shows the correlation between MCS days with the ENSO and IOD indices based on the detrended SST. During the positive phase of ENSO (i.e., El Niño), the western Indian Ocean shows a warmer anomaly (Swapna *et al.*, 2014) and hence is negatively correlated with the MCS days (Figure 7a1), except for the Sumatra region. On the other hand, during the negative phase (i.e., La Niña), most parts of the Indian Ocean experience a cooler anomaly (Benthuysen *et al.*, 2014), and hence are positively correlated (Figure 7a2); the magnitude of correlation is strong in the western Indian Ocean. The western Indian Ocean exhibits anomalous warming during the IOD's positive phase, and hence is negatively correlated with MCS days, whereas the eastern Indian Ocean cools and thus is positively correlated with MCS days (Figure 7a3). In the negative phase, the sign of the SST anomaly reverses, and so does the correlation (Figure 7a4). It can further be argued that when both ENSO and IOD are in the same phase the effects might be amplified/weakened; for example, La Niña and a negative IOD together can augment the MCSs, whereas El Niño and a positive IOD can lead to a decline in MCSs. To explore this further, this study investigated how the proportion of the TIO experiencing different categories of MCS changes in a different regime of ENSO and IOD within the RCP4.5 (Figure 7b) and RCP8.5 (Figure 7c) scenarios. It can be perceived that in both RCPs during the El Niño phase, the proportion of the TIO experiencing different categories of MCS is significantly decreasing, due to the warming. During the La Niña years, not only did the proportion of MCS categories increase, but also higher categories such as Severe and Extreme began to appear. Although the magnitude of the Extreme category proportion is not significant, the Severe category covers a considerable proportion of the TIO. This indicates that La-Niña strengthens the MCS category and

FIGURE 6   Factors responsible for increased (a) sea-surface temperature changes in the atmospheric parameters and (b) changes in the oceanic parameters. SWR: short-wave radiation; LWR: long-wave radiation; LHF: latent heat flux; WS: wind speed; ZADV: zonal advection; MADV: meridional advection. [Colour figure can be viewed at wileyonlinelibrary.com]
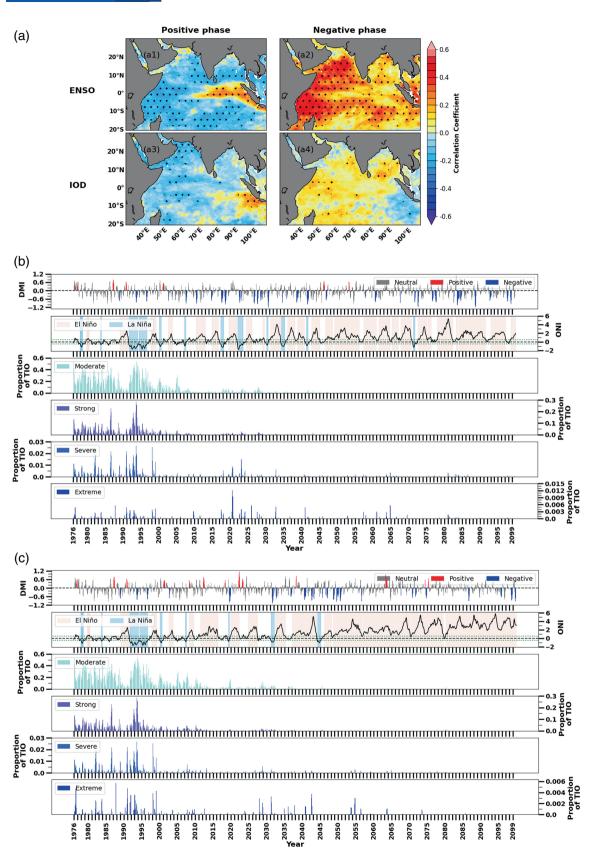
its spatial extent, whereas El Niño weakens both the intensity and spatial extent. Notably, between 1990 and 1995, when La Niña and a negative IOD were both present, a higher proportion of Strong and Severe category MCSs was detected. However, over time, both RCPs show a decrease in the proportion of MCS categories.

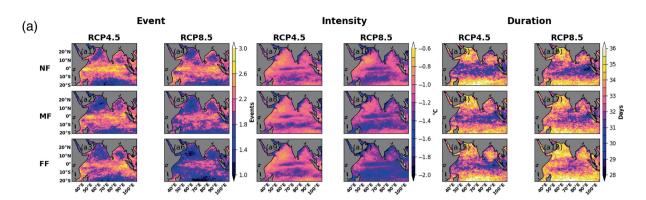## 3.5 | Future MCS metrics with varying baseline period

Figure 8 shows the MCS simulation over the TIO with the varying baseline period. A varying baseline period means the NF MCS is computed by taking the NF period as a
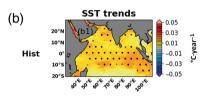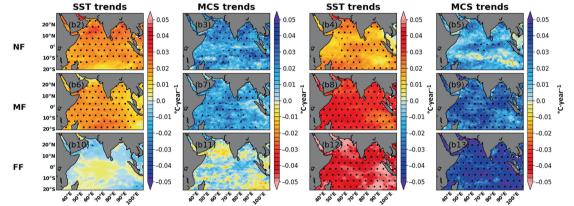
FIGURE 7 (a) Correlation between marine cold spell (MCS) days and climate modes (El Niño–Southern Oscillation [ENSO] and Indian Ocean dipole [IOD]) based on detrended sea-surface temperature. The stippling denotes 95% significance level. (b, c) Impact of ENSO and IOD phases on the proportion of MCS categories for (b) RCP4.5 and (c) RCP8.5 scenarios. DMI: Dipole Mode Index; ONI: Oceanic Nino Index; TIO: tropical Indian Ocean. [Colour figure can be viewed at wileyonlinelibrary.com]
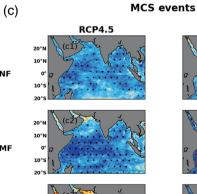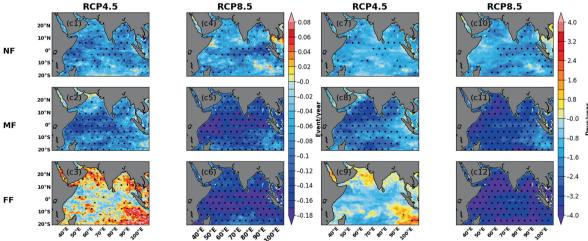
FIGURE 8 (a) Marine cold spell (MCS) metrics with corresponding baseline period in the near future (NF), middle future (MF), and far future (FF). (b) Trends in the future sea-surface temperature (SST) and MCSs computed with corresponding baseline period in the NF, MF, and FF. (c) Trends in MCS event and MCS duration. The stippling denotes 95% significance level. [Colour figure can be viewed at wileyonlinelibrary.com]

baseline, and similarly for the MF and FF. The MCS does not disappear when the corresponding period baseline period is used in the NF, MF, and FF, proving that MCSs are sensitive to the choice of the baseline period. Figure 8a shows that over the AS the number of events is small, the intensity is lower, but the duration is higher. Overall, with few minor changes in magnitude, the spatial signal of MCSs (events, intensity, and duration) remains analogous in all time slices under both RCPs. Figure 8b shows the trends in the SST and MCS intensity; notably, MCS intensities are represented with negative numbers, and hence a positive trend in MCS intensity over time indicates a weakening. The SST continues to increase strongly in both RCPs as we move from the historical period to the future, and consequently the MCS intensity declines, with an exception during the FF in RCP4.5. In RCP4.5, carbon dioxide emissions start to decline after 2045 and will be almost half what they were in 2050 by 2100 (Collins *et al.*, 2013). This explains why in the AS the SST trends fall and the MCS intensity trends climb during the FF period in RCP4.5 Figure 8b10,b11; however, the trends are not statistically significant. The pattern correlation between SST trend and MCS intensity trend ranges between 0.73 and 0.94 in all time frames, with the exception of RCP4.5 in the FF, where it is 0.47 only. This suggests that the MCS is largely sensitive to the deviations in its deriving SST in addition to the choice of baseline period. Figure 8c shows the MCS events and duration had significantly declining trends in all time slices in both RCPs, except for the FF in RCP4.5. In RCP4.5 after the MF period, the degree of warming is not quite as high, and thus the MCS activity is found to be higher in the FF over the AS and BoB; notably, over this location, the trends in duration are not significant.

In summary, adopting a varying baseline period method will not result in the disappearance of MCSs but will instead produce declining trends in MCS activity. This strengthens the fact that though MCSs are sensitive to the chosen baseline period, their activity will still be mostly driven by future SST warming, as shown previously by Oliver (2019) and Wang *et al.* (2022). Moreover, several research questions for additional study will become easily apparent, such as identifying any similarities or discrepancies that persist regardless of the chosen baseline and so forth, which remain a concern for further studies.

4 | CONCLUSION

This study provides future projections of MCSs over the TIO. We employ a fully coupled high-resolution regional Earth system model known as ROM, driven by MPI-ESM-LR (CMIP5), to explore MCS patterns. Specifically, this study delves into how MCS distribution,

intensity, and duration will change from the historical period (1976–2005) and how it will look in the future (2010–2099) under two RCP (RCP4.5 and RCP8.5) emission scenarios, within the context of fixed and varying baseline periods. For the historical period, ROM outperformed the forcing GCM and MEM of the CMIP5 model, confirming its reliability for the future projection of MCSs. Future MCSs have been determined in three time slices; namely, the NF (2010–2039), MF (2040–2069), and FF (2070–2099). Future MCSs with a fixed baseline period reveal that these cold temperature extremes will depart from ~13% (4%), ~56% (66%), and ~69% (93%) of the TIO in the NF, MF, and FF respectively within the RCP4.5 (RCP8.5) scenario. MCS disappearance was first identified in the southern AS in both RCPs, and afterwards, it started to disappear from other TIO locations; finally, MCSs will eventually become a rare event in the future. The genesis and severity of MCSs are influenced by the decrease in net heat flux and increased WS. The investigation of the effect of ENSO and IOD on MCSs reveals that during the El Niño regime, the MCSs declined significantly due to warming. In contrast, the La Niña phase strengthens the MCS intensity as well as increases its spatial extent. The IOD eminently influences the MCSs over the TIO; this is particularly prominent in close proximity to the western and southeastern boxes during its positive and negative phases. This study further investigates the sensitivity of MCSs with the chosen baseline period. Adopting varying baseline periods does not result in the disappearance of MCSs; however, it does produce declining trends in MCS activity.

In conclusion, this study shows the potential of the fully coupled model ROM in simulating MCSs over the TIO. The estimate for the MCSs in this study is based on a single model simulation that shows one potential outcome. An ensemble set of simulations should be taken into consideration together with uncertainty analysis in order to generate far more realistic MCS projections. However, one of the potential benefits of this study's findings can be translated into ecosystem impact assessment and its management by considering the changes in these extremes. As well as how these extremes may play a role in offsetting the impacts of MHWs and act as a potential buffer against ongoing warming. However, further study is needed by considering such features as the choice of the baseline period and the the acute and chronic impacts of MCSs.

CONFLICT OF INTEREST STATEMENT
The authors declare that they have no known conflict of interest that could have influenced the work reported in this article.

DATA AVAILABILITY STATEMENT
Publicly available NOAA OISST V2 daily SST data are obtained from NOAA's Physical Science Laboratory (https://psl.noaa.gov/data/gridded/data.noaa.oisst.v2.highres.html). The CMIP5 model data are available from https://esgf-node.llnl.gov/search/. ROM-simulated data would be made available upon request to the corresponding author.

ORCID
Pankaj Kumar https://orcid.org/0000-0003-1906-9852
Alok Kumar Mishra https://orcid.org/0000-0002-1718-0437

REFERENCES
Alexander, L.V., Zhang, X., Peterson, T.C., Caesar, J., Gleason, B., Klein Tank, A.M.G. et al. (2006) Global observed changes in daily climate extremes of temperature and precipitation. *Journal of Geophysical Research: Atmospheres*, 111(D5). Available from: https://doi.org/10.1029/2005JD006290

Amaya, D.J., Jacox, M.G., Fewings, M.R., Saba, V.S., Stuecker, M.F., Rykaczewski, R.R. et al. (2023) Marine heatwaves need clear definitions so coastal communities can adapt. *Nature*, 616(7955), 29–32.

Benthuysen, J., Feng, M. & Zhong, L. (2014) Spatial patterns of warming off Western Australia during the 2011 Ningaloo Niño: Quantifying impacts of remote and local forcing. *Continental Shelf Research*, 91, 232–246. Available from: https://doi.org/10.1016/j.csr.2014.09.014

Burgess, S.N., McCulloch, M.T., Mortimer, G.E. & Ward, T.M. (2009) Structure and growth rates of the high-latitude coral: Plesiastrea versipora. *Coral Reefs*, 28, 1005–1015.

Cahyarini, S.Y., Pfeiffer, M., Reuning, L., Liebetrau, V., Dullo, W.C., Takayanagi, H. et al. (2021) Modern and sub-fossil corals suggest reduced temperature variability in the eastern pole of the Indian Ocean dipole during the medieval climate anomaly. *Scientific Reports*, 11(1), 14952.

Chiswell, S.M. & O'Callaghan, J.M. (2021) Long-term trends in the frequency and magnitude of upwelling along the west coast of the South Island, New Zealand, and the impact on primary production. *New Zealand Journal of Marine and Freshwater Research*, 55(1), 177–198.

Collins, M., Knutti, R., Arblaster, J., Dufresne, J.L., Fichefet, T., Friedlingstein, P. et al. (2013) Long-term climate change: projections, commitments and irreversibility.

Darmaraki, S., Somot, S., Sevault, F., Nabat, P., Cabos Narvaez, W.D., Cavicchia, L. et al. (2019) Future evolution of marine heatwaves in the Mediterranean Sea. *Climate Dynamics*, 53, 1371–1392.

Dinesh, A.S., Mishra, A.K., Dubey, A.K., Kumari, S. & Anand, A. (2023) Comparative changes in seasonal marine heatwaves and cold spells over the tropical Indian Ocean during recent decades and disentangling the drivers of highly intense events. *International Journal of Climatology*, 43(15), 7428–7446.

Donders, T.H., de Boer, H.J., Finsinger, W., Grimm, E.C., Dekker, S.C., Reichart, G.J. et al. (2011) Impact of the Atlantic warm Pool on precipitation and temperature in Florida during North Atlantic cold spells. *Climate Dynamics*, 36, 109–118.

Du, Y., Xie, S.P., Huang, G. & Hu, K. (2009) Role of air–sea interaction in the long persistence of El Niño–induced north Indian Ocean warming. *Journal of Climate*, 22(8), 2023–2038.

Dubey, A.K. & Kumar, P. (2023) Future projections of heatwave characteristics and dynamics over India using a high-resolution regional earth system model. *Climate Dynamics*, 60(1–2), 127–145.

Dubey, A.K., Lal, P., Kumar, P., Kumar, A. & Dvornikov, A.Y. (2021) Present and future projections of heatwave hazard-risk over India: a regional earth system model assessment. *Environmental Research*, 201, 111573.

Dwivedi, S., Mishra, A.K. & Srivastava, A. (2019) Upper ocean high resolution regional modeling of the Arabian Sea and bay of Bengal. *Acta Oceanologica Sinica*, 38, 32–50.

Dwivedi, S., Srivastava, A. & Mishra, A.K. (2018) Upper ocean four-dimensional variational data assimilation in the Arabian Sea and bay of Bengal. *Marine Geodesy*, 41(3), 230–257.

Frölicher, T.L., Fischer, E.M. & Gruber, N. (2018) Marine heatwaves under global warming. *Nature*, 560(7718), 360–364.

Gilmore, R.G., Bullock, L.H. & Berry, F.H. (1978) Hypothermal mortality in marine fishes of south-central Florida, January, 1977. *Gulf of Mexico Science*, 2(2), 1.

Giorgi, F. (2019) Thirty years of regional climate modeling: where are we and where are we going next? *Journal of Geophysical Research: Atmospheres*, 124(11), 5696–5723.

González-Espinosa, P.C. & Donner, S.D. (2020) Predicting cold-water bleaching in corals: role of temperature, and potential integration of light exposure. *Marine Ecology Progress Series*, 642, 133–146.

Grant, P.R., Grant, B.R., Huey, R.B., Johnson, M.T., Knoll, A.H. & Schmitt, J. (2017) Evolution caused by extreme events. *Philosophical Transactions of the Royal Society B: Biological Sciences*, 372(1723), 20160146.

Gunter, G. (1951) Destruction of fishes and other organisms on the south Texas coast by the cold wave of January 28-February 3, 1951. *Ecology*, 32(4), 731–736.

Hagemann, S. & Dümenil, L. (1997) A parametrization of the lateral waterflow for the global scale. *Climate Dynamics*, 14, 17–31.

Heron, S.F., Willis, B.L., Skirving, W.J., Eakin, C.M., Page, C.A. & Miller, I.R. (2010) Summer hot snaps and winter conditions: modelling white syndrome outbreaks on great barrier reef corals. *PLoS One*, 5(8), e12210.

Hibler, W.D. (1979) A dynamic Thermodynamic Sea ice model. *Journal of Physical Oceanography*, 9, 815–846. Available from: https://doi.org/10.1175/1520-0485(1979)009

Hicks, D. & McMahon, R. (2002) Temperature acclimation of upper and lower thermal limits and freeze resistance in the nonindigenous brown mussel, *Perna perna* (L.), from the Gulf of Mexico. *Marine Biology*, 140, 1167–1179.

Hobday, A.J., Alexander, L.V., Perkins, S.E., Smale, D.A., Straub, S.C., Oliver, E.C. et al. (2016) A hierarchical approach to defining marine heatwaves. *Progress in Oceanography*, 141, 227–238.

Holbrook, N.J., Scannell, H.A., Sen Gupta, A., Benthuysen, J.A., Feng, M., Oliver, E.C. et al. (2019) A global assessment of marine heatwaves and their drivers. *Nature Communications*, 10(1), 2624.

Holt, S.A. & Holt, G.J. (1983) Cold death of fishes at Port Aransas, Texas: January 1982. *The Southwestern Naturalist*, 28(4), 464–466.

Hurst, T.P. (2007) Causes and consequences of winter mortality in fishes. *Journal of Fish Biology*, 71(2), 315–345.

IPCC. (2019). The ocean and cryosphere in a changing climate. In: H.-O. Pörtner, D.C. Roberts, V. Masson-Delmotte, P. Zhai, M. Tignor, E. Poloczanska, K. Mintenbeck, A. Alegría, M. Nicolai, A. Okem, J. Petzold, B. Rama, N. M. Weyer (Eds.). *IPCC Special Report on the Ocean and Cryosphere in a Changing Climate*. Cambridge, UK: Cambridge University Press. Available from: https://doi.org/10.1017/9781009157964.

Jacob, D. & Podzun, R. (1997) Sensitivity studies with the regional climate model REMO. *Meteorology and Atmospheric Physics*, 63, 119–129.

Jacob, D., Van den Hurk, B.J.J.M., Andrae, U., Elgered, G., Fortelius, C., Graham, L.P. et al. (2001) A comprehensive model inter-comparison study investigating the water budget during the BALTEX-PIDCAP period. *Meteorology and Atmospheric Physics*, 77, 19–43.

Jungclaus, J.H., Fischer, N., Haak, H., Lohmann, K., Marotzke, J., Matei, D. et al. (2013) Characteristics of the ocean simulations in the max Planck Institute Ocean model (MPIOM) the ocean component of the MPI-earth system model. *Journal of Advances in Modeling Earth Systems*, 5(2), 422–446.

Kumar, P., Javed, A., Kolli, R.K., Sachan, D., Dinesh, A.S., Murukesh, M. et al. (2023) National Colloquium for advances in weather and climate prediction and climate change projection over South Asia: applications in water and agriculture sectors. *Bulletin of the American Meteorological Society*, 104(9), E1564–E1569.

Kumar, P., Mishra, A.K., Dubey, A.K., Javed, A., Saharwardi, M.S., Kumari, A. et al. (2022) Regional earth system modelling framework for CORDEX-SA: an integrated model assessment for Indian summer monsoon rainfall. *Climate Dynamics*, 59(7–8), 2409–2428.

Kumar, P., Sein, D., Cabos, W. & Jacob, D. (2014a) Improved precipitation extremes and climatology in a regional coupled model simulation over CORDEX south Asia domain. *AGU Fall Meeting Abstracts*, 2014, A53Q-07.

Kumar, P., Sein, D., Cabos, W. & Jacob, D. (2014b) Improvement of simulated monsoon precipitation over South-Asia with a regionally coupled model ROM. In: Bärring, L., Reckermann, M., Rockel, B. & Rummukain, M. (Eds.) *3rd International Lund Regional-Scale Climate Modelling Workshop 21st Century Challenges in Regional Climate Modelling: Workshop proceedings*. Lund, Sweden, 16-19 June 2014, (International Baltic Earth

Secretariat Publications; 3): International Baltic Earth Secretariat, p. 434.

Kumari, A. & Kumar, P. (2023) Evaluation and future projection of the extreme precipitation over India and its homogeneous regions: a regional earth system model perspective. *International Journal of Climatology*, 43, 3679–3697.

Li, J. & Su, J. (2020) Comparison of Indian Ocean warming simulated by CMIP5 and CMIP6 models. *Atmospheric and Oceanic Science Letters*, 13(6), 604–611.

Lirman, D., Schopmeyer, S., Manzello, D., Gramer, L.J., Precht, W.F., Muller-Karger, F. et al. (2011) Severe 2010 cold-water event caused unprecedented mortality to corals of the Florida reef tract and reversed previous survivorship patterns. *PLoS One*, 6(8), e23047.

Marsland, S.J., Haak, H., Jungclaus, J.H., Latif, M. & Röske, F. (2003) The max-Planck-institute global ocean/sea ice model with orthogonal curvilinear coordinates. *Ocean Modelling*, 5(2), 91–127.

McEachron, L.W., Matlock, G.C., Bryan, C.E., Unger, P., Cody, T.J. & Martin, J.H. (1994) Winter mass mortality of animals in Texas bays. *Gulf of Mexico Science*, 13(2), 6.

Mintenbeck, K. (2017) Impacts of Climate Change on the Southern Ocean. In: Phillips, B. & Pérez-Ramírez, M. (Eds.) *Climate Change Impacts on Fisheries and Aquaculture: A Global Analysis, Climate Change Impacts on Fisheries and Aquaculture: A Global Analysis*. Wiley-Blackwell. Available from: https://doi.org/10.1002/9781119154051.ch20

Mishra, A.K., Dubey, A.K. & Dinesh, A.S. (2023) Diagnosing whether the increasing horizontal resolution of regional climate model inevitably capable of adding value: investigation for Indian summer monsoon. *Climate Dynamics*, 60(7–8), 1925–1945.

Mishra, A.K., Dwivedi, S. & Di Sante, F. (2021a) Performance of the RegCM-MITgcm coupled regional model in simulating the Indian summer monsoon rainfall. *Pure and Applied Geophysics*, 178, 603–617.

Mishra, A.K., Kumar, P., Dubey, A.K., Javed, A., Saharwardi, M.S., Sein, D.V. et al. (2021b) Impact of horizontal resolution on monsoon precipitation for CORDEX-South Asia: a regional earth system model assessment. *Atmospheric Research*, 259, 105681.

Mishra, A.K., Kumar, P., Dubey, A.K., Jha, S.K., Sein, D.V. & Cabos, W. (2022) Demonstrating the asymmetry of the Indian Ocean dipole response in regional earth system model of CORDEX-SA. *Atmospheric Research*, 273, 106182.

Moore, R.H. (1976) Observations on fishes killed by cold at Port Aransas, Texas, 11-12 January 1973. *The Southwestern Naturalist*, 20, 461–466.

Morgan, R., Finnøen, M.H., Jensen, H., Pélabon, C. & Jutfelt, F. (2020) Low potential for evolutionary rescue from climate change in a tropical fish. *Proceedings of the National Academy of Sciences*, 117(52), 33365–33372.

Oliver, E.C. (2019) Mean warming not variability drives marine heatwave trends. *Climate Dynamics*, 53(3–4), 1653–1659.

Oliver, E.C., Benthuysen, J.A., Darmaraki, S., Donat, M.G., Hobday, A.J., Holbrook, N.J. et al. (2021) Marine heatwaves. *Annual Review of Marine Science*, 13, 313–342.

Oliver, E.C., Burrows, M.T., Donat, M.G., Sen Gupta, A., Alexander, L.V., Perkins-Kirkpatrick, S.E. et al. (2019) Projected marine heatwaves in the 21st century and the potential for ecological impact. *Frontiers in Marine Science*, 6, 734.

Pandey, L.K. & Dwivedi, S. (2021) Comparing the performance of turbulent kinetic energy and K-profile parameterization vertical parameterization schemes over the tropical Indian Ocean. *Marine Geodesy*, 44(1), 42–69.

Pandey, L.K., Dwivedi, S. & Martin, M. (2021) Short-term predictability of the bay of Bengal region using a high-resolution Indian ocean model. *Marine Geodesy*, 44(3), 215–237.

Plecha, S.M. & Soares, P.M. (2020) Global marine heatwave events using the new CMIP6 multi-model ensemble: from shortcomings in present climate to future projections. *Environmental Research Letters*, 15(12), 124058.

Reynolds, R.W., Smith, T.M., Liu, C., Chelton, D.B., Casey, K.S. & Schlax, M.G. (2007) Daily high-resolution-blended analyses for sea surface temperature. *Journal of Climate*, 20(22), 5473–5496.

Roxy, M.K., Ritika, K., Terray, P. & Masson, S. (2014) The curious case of Indian Ocean warming. *Journal of Climate*, 27(22), 8501–8509.

Saharwardi, M.S., Kumar, P. & Sachan, D. (2022) Evaluation and projection of drought over India using high-resolution regional coupled model ROM. *Climate Dynamics*, 58(1), 503–521.

Saji, N.H., Goswami, B.N., Vinayachandran, P.N. & Yamagata, T. (1999) A dipole mode in the tropical Indian Ocean. *Nature*, 401(6751), 360–363.

Saranya, J.S., Roxy, M.K., Dasgupta, P. & Anand, A. (2022) Genesis and trends in marine heatwaves over the tropical Indian Ocean and their interaction with the Indian summer monsoon. *Journal of Geophysical Research: Oceans*, 127(2), e2021JC017427.

Sayantani, O. & Gnanaseelan, C. (2015) Tropical Indian Ocean subsurface temperature variability and the forcing mechanisms. *Climate Dynamics*, 44, 2447–2462.

Schlegel, R.W., Darmaraki, S., Benthuysen, J.A., Filbee-Dexter, K. & Oliver, E.C. (2021) Marine cold-spells. *Progress in Oceanography*, 198, 102684.

Sein, D.V., Dvornikov, A.Y., Martyanov, S.D., Cabos, W., Ryabchenko, V.A., Gröger, M. et al. (2022) Indian Ocean marine biogeochemical variability and its feedback on simulated South Asia climate. *Earth System Dynamics*, 13(2), 809–831.

Sein, D.V., Gröger, M., Cabos, W., Alvarez-Garcia, F.J., Hagemann, S., Pinto, J.G. et al. (2020) Regionally coupled atmosphere-ocean-marine biogeochemistry model ROM: 2. Studying the climate change signal in the North Atlantic and Europe. *Journal of Advances in Modeling Earth Systems*, 12(8), e2019MS001646.

Sein, D.V., Mikolajewicz, U., Gröger, M., Fast, I., Cabos, W., Pinto, J.G. et al. (2015) Regionally coupled atmosphere-ocean-sea ice-marine biogeochemistry model ROM: 1. *Description and Validation. Journal of Advances in Modeling Earth Systems*, 7(1), 268–304.

Sen Gupta, A., Thomsen, M., Benthuysen, J.A., Hobday, A.J., Oliver, E., Alexander, L.V. et al. (2020) Drivers and impacts of the most extreme marine heatwaves events. *Scientific Reports*, 10, 19359.

Seneviratne, S., Nicholls, N., Easterling, D., Goodess, C., Kanae, S., Kossin, J. et al. (2012) Changes in climate extremes and their impacts on the natural physical environment.

Seneviratne, S.I., Zhang, X., Adnan, M., Badi, W., Dereczynski, C., Di Luca, A. et al. (2021) Weather and climate extreme events in a changing climate (Chapter 11). In IPCC Sixth Assessment Report.

Smale, D.A., Wernberg, T., Oliver, E.C., Thomsen, M., Harvey, B.P., Straub, S.C. et al. (2019) Marine heatwaves threaten global biodiversity and the provision of ecosystem services. *Nature Climate Change*, 9(4), 306–312.

Smith, M.D. (2011) The ecological role of climate extremes: current understanding and future prospects. *Journal of Ecology*, 99(3), 651–655.

Srivastava, A., Dwivedi, S. & Mishra, A.K. (2016) Intercomparison of high-resolution bay of Bengal circulation models forced with different winds. *Marine Geodesy*, 39(3–4), 271–289.

Swapna, P., Krishnan, R. & Wallace, J.M. (2014) Indian Ocean and monsoon coupled interactions in a warming environment. *Climate Dynamics*, 42(9), 2439–2454.

Tobin, S. (2020) Seasonal climate summary for the southern hemisphere (spring 2017): equal-fifth warmest spring on record, with rainfall mixed. *Journal of Southern Hemisphere Earth Systems Science*, 70(1), 304–327.

Veytia, D., Corney, S., Meiners, K.M., Kawaguchi, S., Murphy, E.J. & Bestley, S. (2020) Circumpolar projections of Antarctic krill growth potential. *Nature Climate Change*, 10(6), 568–575.

Vialard, J. & Delecluse, P. (1998) An OGCM study for the TOGA decade. Part II: barrier-layer formation and variability semantic scholar. *Journal of Physical Oceanography*, 28(6), 1071–1088.

Vialard, J., Menkes, C., Boulanger, J.P., Delecluse, P., Guilyardi, E., McPhaden, M.J. et al. (2001) A model study of oceanic mechanisms affecting equatorial Pacific sea surface temperature during the 1997–98 El Niño. *Journal of Physical Oceanography*, 31(7), 1649–1675.

Wang, Y., Kajtar, J.B., Alexander, L.V., Pilo, G.S. & Holbrook, N.J. (2022) Understanding the changing nature of marine cold-spells. *Geophysical Research Letters*, 49(6), e2021GL097002.

Wells, H.W., Wells, M.J. & Gray, I.E. (1961) Winter fish mortality in Pamlico sound, North Carolina. *Ecology*, 42(1), 217–219.